MOX-Report No. 32/2016

Statistical Assessment and Calibration of Numerical ECG Models

Tarabelloni, N.; Schenone, E.; Collin, A.; Ieva, F.; Paganoni, A.M.; Gerbeau, J.-F.

MOX, Dipartimento di Matematica
Politecnico di Milano, Via Bonardi 9 - 20133 Milano (Italy)

mox-dmat@polimi.it http://mox.polimi.it

STATISTICAL ASSESSMENT AND CALIBRATION OF NUMERICAL ECG MODELS

N. TARABELLONI, E. SCHENONE, A. COLLIN, F. IEVA, A.M. PAGANONI, AND J.-F. GERBEAU

Abstract. Objective: Because of the inter-subject variability of ECGs in a healthy population, it is not straightforward to assess the quality of synthetic ECGs produced by deterministic mathematical models. We propose a statistical method to address this question.

Methods: We use a dataset of 1588 healthy, real ECGs and we introduce a way to calibrate the deterministic model so that its output fits the dataset. Our approach is based on the concepts of spatial quantiles and spatial depths. These notions are convenient to manipulate functional data since they provide a non-parametric way to measure the discrepancy of the model output with a distribution of data.

Results: The method is successfully applied to two very different models: a phenomenological model based on ordinary differential equations, and a complex biophysical model based on partial differential equations set on a three-dimensional geometry of the heart and the torso. We show in particular that the proposed calibration strategy allows us to improve the quality of the ECG obtained with the biophysical model.

Significance: The proposed methodology is to our knowledge the first attempt to assess the quality of synthetic ECGs with quantitative statistical arguments. More generally it can be applied to other situations where a deterministic model produces a functional output that has to be compared with a population of measurements containing inter-subject variability.

1. Introduction

The generation of synthetic electrocardiograms (ECGs) by computer simulations has been the object of many studies. The models can be based on ordinary differential equations (ODEs) (McSharry et al., 2003; Clifford et al., 2005), on three-dimensional cellular automata (Wei et al., 1995), or on three-dimensional partial differential equations (PDEs) (Potse et al., 2003, 2009; Trudel et al., 2004; Boulakia et al., 2010; Martin et al., 2012). These approaches are motivated by different problems: for example, the smoothing of real data (Clifford et al., 2005), the assessment of cardiac simulations and the evaluation of modeling hypotheses (Potse et al., 2014), the resolution of the inverse problem of electrocardiography through parameter identification of a forward model (Rincon et al., 2013; Boulakia et al., 2012; Corrado et al., 2015).

One of the difficulties to assess and to calibrate those models stems from the variability of the real ECGs: many different ECGs can be observed in different

Key words and phrases. Electrocardiograms, statistical assessment, Functional Data Analysis, model calibration, depth measures.

healthy subjects. The calibration of a synthetic ECG should therefore not be done with respect to one specific measurement, as it is typically done for engineering problems, but rather with respect to a population of measurements.

In this paper, we propose an original statistical strategy to address this problem and we illustrate it on two very different models of ECGs. The database used for the calibration is made of 1588 real, healthy ECGs.

When the calibration is done on a population of measurements, the distribution of observations in the sample is an important information. In order to model the randomness of the reference output, it could be useful to gather information on the probability distribution of data. But, since our data are functions, this would require to work with probability distributions on functional spaces, i.e. infinite-dimensional spaces. To avoid this difficulty, we used the concepts of spatial depth and spatial quantiles (Chaudhuri, 1996; Chakraborty and Chaudhuri, 2014), which are non-parametric tools. The proposed methodology is of course not limited to ECGs. It can be typically used to calibrate a deterministic model whose output is a function which has to be compared to a population of measurements.

The article is organized as follows. The general methodology is presented in Section 2: Section 2.1.1 and Section 2.1.2 are devoted to a brief presentation of the ODE and the PDE models, respectively; the statistical framework of Functional Data Analysis and the calibration problem are presented in Section 2.2; an overview of the real dataset of ECG signals used to carry out the calibration is proposed 2.3. In Section 3 the results obtained with the ODE and PDE models are presented. A discussion is proposed in Section 4, and a some concluding remarks in Section 5.

2. Methods and Materials

2.1. **ECG Models.** In this section we briefly introduce the mathematical models describing human ECGs which will be used in the following to illustrate the calibration strategy.

2.1.1. *A Model Based on Ordinary Differential Equations.* Here we describe a deterministic model based on a ODE system reproducing lead I of an ECG signal. This model was first proposed in McSharry et al. (2003) and then refined in Clifford et al. (2005) in order to provide a simple yet effective way to simulate synthetic ECG signals. It was also employed to filter out noise from raw ECG measurements (Clifford et al., 2005). It is based on a phenomenological ODE system yielding a morphologically valid ECG shape.

In its general form, the model describes the ECG as a set of 5 deflections corresponding to the P, Q, R, S and T waves. It generates a trajectory in the three-dimensional state-space with coordinates (x, y, z), whose periodicity is reflected by the movement of the trajectory around an attracting limit cycle of unit radius in the $x - y$ plane. The model reads:

$$
(1) \qquad \begin{cases} \dot{x} = \alpha x - \omega y \\ \dot{y} = \alpha y + \omega x \\ \dot{z} = -\sum_{i=1}^{5} a_i \Delta\theta_i \exp\left(-\frac{\Delta\theta_i^2}{2b_i^2}\right) - (z - z_0) \end{cases}
$$

with initial state $(-1, 0, 0)$, where $\alpha = 1 - \sqrt{x^2 + y^2}$, $\Delta\theta_i = \theta - \theta_i \mod 2\pi$, $\theta = \text{atan2}(y, x)$ (the fourth quadrant arctangent of x and y, with $-\pi \leq \text{atan2}(y, x) \leq \pi$, $\omega = 2\pi/T$, having the meaning of angular velocity, is obtained by signal's period T and the index i spans over the 5 waves of the ECG mentioned above. The parameters to be chosen are the triplets (a_i, θ_i, b_i) for each of the 5 waves for a total of 15 parameters.

The ECG signal is then obtained by computing $z(t)$. The quantity $z - z_0$ is a shifting term, where for instance z_0 can be taken as a sinusoidal wave, acting as a baseline correction. Since the real data we are going to use in the ECG application have already been corrected for this baseline, such a term is not needed in our model, thus we take $z - z_0 = 0$. We can resort to a cylindric coordinate representation of the dynamical system, then after integrating the z equation with respect to θ, we get:

$$
(2) \qquad z(\theta) = \sum_{i=1}^{5} \frac{a_i b_i^2}{\omega} \exp\left(-\frac{\Delta\theta_i^2}{2b_i^2}\right), \quad \theta = \omega t - \pi.
$$

2.1.2. *A Model Based on Partial Differential Equations.* To illustrate the versatility of the approach proposed in this study, we consider another way to generate synthetic ECGs. Contrary to the previous one, the purpose here is no longer to mimic the ECG curves with a low-complexity dynamical system, but to use biophysical equations to model the electrophysiology of the cells, the myocardium and the torso. We summarize here the main features of the model, and we refer to Schenone et al. (2015) for more details.

In the ventricles, we use the standard bidomain equations (Sachse, 2004; Sundnes et al., 2006). Denoting by u_e, u_i and $V_m = u_i - u_e$ the extracellular, the intracellular and the transmembrane potential respectively, we have:

$$
(3) \qquad \begin{cases} A_m\left(C_m \dfrac{\partial V_m}{\partial t} + I_{ion}^{MV}(V_m, w_1, \ldots, w_n)\right) \\ \qquad - \operatorname{div}\left(\vec{\vec{\sigma}}_i \cdot \vec{\nabla} V_m\right) = \operatorname{div}\left(\vec{\vec{\sigma}}_i \cdot \vec{\nabla} u_e\right) + A_m I_{app}, \\ \operatorname{div}\left(\left(\vec{\vec{\sigma}}_i + \vec{\vec{\sigma}}_e\right) \cdot \vec{\nabla} u_e\right) = -\operatorname{div}\left(\vec{\vec{\sigma}}_i \cdot \vec{\nabla} V_m\right), \end{cases}
$$

in $\mathcal{B} \times (0, T)$, where $\mathcal{B}$ denotes the domain occupied by the ventricles, A_m the ratio of membrane area per unit volume, C_m the membrane capacitance per unit surface and I_{app} a given applied stimulus current. The current I_{ion}^{MV} is defined by the minimal ventricular (MV) model (Bueno-Orovio et al., 2008). The conductivity tensors $\vec{\vec{\sigma}}_i$ and $\vec{\vec{\sigma}}_e$ are defined by $\vec{\vec{\sigma}}_{i,e} = \sigma_{i,e}^{v,t} \vec{\vec{I}} + (\sigma_{i,e}^{v,l} - \sigma_{i,e}^{v,t}) \vec{\tau} \otimes \vec{\tau}$, where $\vec{\vec{I}}$ denotes the three-dimensional identity matrix, the vector $\vec{\tau}$ is of unit length and parallel to the local fiber direction, and $\sigma_{i,e}^{v,l}$ and $\sigma_{i,e}^{v,t}$ are respectively the conductivity

coefficients in the intra- and extra-cellular ventricular medium measured along and across the fiber direction.

For the atria, we use a surface model derived by asymptotic analysis from the volume bidomain model. Once introduced the formalism needed to write the partial differential equations on a two-dimensional manifold, the model is similar to (3). We refer to Chapelle et al. (2013) and Collin et al. (2013) for its precise form. Here we just emphasize that, even if it is set on the midsurface, it actually takes into account volume effects, like the anisotropy variations across the thickness. Indeed, the intra- and extra-cellular diffusion tensors $\underline{\underline{\sigma}}_i$ and $\underline{\underline{\sigma}}_e$ are defined by

$$\underline{\underline{\sigma}}_{i,e} = \sigma_{i,e}^{a,t}\underline{\underline{I}} + (\sigma_{i,e}^{a,l} - \sigma_{i,e}^{a,t})\big[I_0(\theta)\underline{\tau}_0 \otimes \underline{\tau}_0 + J_0(\theta)\underline{\tau}_0^{\perp} \otimes \underline{\tau}_0^{\perp}\big], \tag{4}$$

where $\underline{\underline{I}}$ denotes the identity tensor in the tangential plane, $\underline{\tau}_0$ is a unit vector parallel to the local fiber direction on the atria midsurface. The variation of the fibers through the thickness of the atria is modeled by the terms $I_0(\theta) = \frac{1}{2} + \frac{1}{4\theta}\sin(2\theta)$ and $J_0(\theta) = 1 - I_0(\theta)$. The cell activity in the atria is described with the Courtemanche-Ramirez-Nattel ionic model (Courtemanche et al., 1998). The fast conduction regions in the atria (Bachmann bundle, *crista terminalis*, pectinate muscles) and the low conduction regions (*fossa ovalis*) are modeled by modifying the maximum conductance of the sodium channel. The two atria are connected by the Bachmann bundle and the *fossa ovalis*. The fibrous skeleton which separates the atria and the ventricles is modeled with a thin layer where the intracellular conductivity is set to zero and the extracellular conductivity is very low. In the ventricle, the Purkinje fibers are roughly modeled with a predefined stimulus pattern which lasts 5 ms.

To obtain an electrocardiogram, the volume and surface bidomain equations are coupled with a Poisson problem in the torso Ω_T:

$$-\operatorname{div}(\sigma_T \vec{\nabla} u_T) = 0, \tag{5}$$

where the electrical conductivity σ_T takes different scalar values in the ribs, the lungs, and the remaining part of the torso (Buist and Pullan, 2003). For the transmission conditions at the heart-body interface $\partial\Omega_H$, we assume that the extracellular current does not flow through the pericardium (isolated heart assumption) and we consider a resistor-capacitor conditions (Boulakia et al., 2010; Schenone et al., 2015).
Then the numerical ECG is obtained by extracting the values of u_T in the standard locations of the electrode leads (Malmivuo and Plonsey, 1995) (see e.g. the first lead in Fig. 1). In Schenone et al. (2015), the ECGs obtained with this approach have been assessed with respect to several qualitative and quantitative criteria (QRS and ST segment duration, wave orientation and amplitude, *etc.*), both in healthy and pathological cases. The pathologies considered were the ventricular bundle blocks, the Bachmann's bundle blocks and the Wolff-Parkinson-White syndrome.

2.2. **Statistical Calibration.** ECGs are data in form of functions, and as such they can be conveniently interpreted within the recent and growing statistical framework of Functional Data Analysis (FDA). Functional data generally describe the evolution of quantities of interest depending on a continuous variable (the time in our

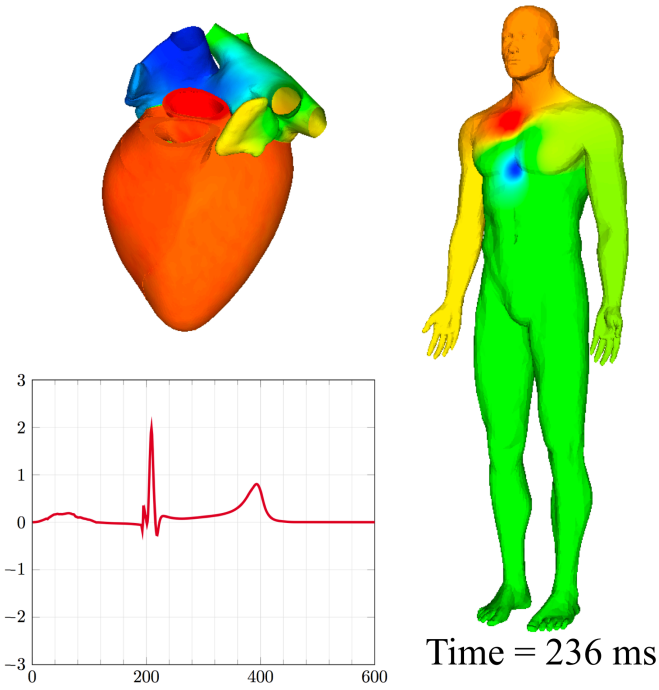

FIGURE 1. Numerical ECG obtained with the three-dimensional biophysical model (section 2.1.2). *Top left*: the heart geometry. *Left*: the first lead of the ECG. *Right*: the body surface potential.

case). Our assessment and calibration strategy will be directly settled within the FDA framework.

Though keeping some similarities with classic concepts of standard multivariate statistics, functional data are structurally different both from a mathematical and empirical perspective. The most important difference is that functional data are sample observations of random functions, i.e. random elements of Hilbert spaces, rather than the Euclidean space $\mathbb{R}^d$. Hence proper statistical tools have to be introduced to underpin their analysis. In the following, we will consider random processes of the form $X : (\Omega, \mathcal{B}, \mathbb{P}) \longrightarrow (\mathcal{V}, \|\cdot\|)$ where $(\Omega, \mathcal{B}, \mathbb{P})$ is a probability space and $\mathcal{V}$ denotes a real separable Hilbert space, with norm $\|\cdot\|$ and scalar product $\langle\cdot,\cdot\rangle$. For all $\omega \in \Omega$, X_ω denotes the function $t \longmapsto X(\omega, t)$, which is an element of $\mathcal{V}$.

2.2.1. *Spatial Quantiles.* Quantiles are of great importance for functional data, since they provide direct, non-parametric information on the distribution of data, without assumptions which could be difficult to prove in practice.

Spatial quantiles, a particular type of M-quantiles (Koltchinskii, 1997), were originally proposed for multivariate data (Chaudhuri, 1996) and then generalized to functional data in separable Hilbert spaces (Chakraborty and Chaudhuri, 2014). For a random function $X \in \mathcal{V}$ and $u \in \mathcal{V}$ s.t. $\|u\| < 1$, the *spatial* $u-$*quantile* of

X is the solution of the problem

$$\textbf{(Q)} \qquad Q_X(u) := \underset{Q \in \mathcal{V}}{\arg\min} \left\{ \mathbb{E}\left[\|X - Q\| - \|X\| \right] - \langle u, Q \rangle \right\}.$$

To give a more intuitive understanding of $Q_X(u)$, let us consider the case of a real random variable (r.v.) and show that this definition generalizes the standard notion of univariate quantiles. Let Y be a continuous, real r.v. with cumulative distribution function F_Y, and $u = 2\alpha - 1$, with $\alpha \in (0, 1)$. Then:

$$Q_Y(u) = \underset{Q \in \mathbb{R}}{\arg\min}\, \mathbb{E}\left(|Y - Q| - |Y| - Q(2\alpha - 1) \right),$$

and by differentiation

$$2\alpha - 1 = -\mathbb{E}\frac{Y - Q_Y(u)}{|Y - Q_Y(u)|} = 2F_Y(Q_Y(u)) - 1,$$

from which $F_Y(Q_Y(u)) = \alpha$, hence $Q_Y(u)$ is the α-th quantile of Y. In particular, if $u = 0$ then $Q_Y(0)$ is the usual median of Y. In view of this, the standard one-dimensional quantiles can be re-indexed by u so that they are centered on the median and that outlyingness corresponds to a signed increase of u towards -1 or $+1$.

In view of this, the choice $u = 0$ in **(Q)** gives the *spatial median* of X, in analogy with the scalar case. The spatial median was introduced long before the spatial quantiles in the context robust statistics (see Kemperman, 1987). It enjoys some of the classical and attractive properties of the usual median, like robustness (50% breakdown point) or the fact that for symmetric distributions of X around a point m (i.e. $X - m \sim -X + m$), it coincides with m.

Consider now the case of $u \in \mathcal{V}$, $\|u\| < 1$ and $u \neq 0$, then the norm $\|u\| \in (0, 1)$ gives a measure of outlyingness of $Q_X(u)$ along the direction $u/\|u\|$ or, in other words, it expresses the order of the $u-$quantile $Q_X(u)$.

2.2.2. *The Calibration Method.* For the sake of clarity, the model is denoted by the map $\mathcal{M} : \Theta \subset \mathbb{R}^d \to \mathcal{V}$, where Θ is the parameter domain. The output of the model with respect to the parameters θ is a function $t \mapsto f_\theta(t)$. This is denoted by $\mathcal{M}(\theta) = f_\theta$. Without loss of generality we denoted by t the continuous variable of the functional output, which can be thought of as time.

We assume to have a dataset of N functional data, $\mathcal{D} = \{X_1, X_2, \ldots, X_N\}$, where the X_i are functions of t. As an example, $\mathcal{D}$ may be a database of empirical measurements of the output of the process (like in our application to ECGs), a dataset of measurements used for benchmark purposes, or just a set of representative solutions corresponding to some configurations of interest of the model.

Given a $u \in \mathcal{V}$, with $\|u\| < 1$, our calibration procedure consists in solving the following problem:

$$\textbf{(C)} \qquad \theta_u^* := \underset{\theta \in \Theta}{\arg\min} \left\{ \mathbb{E}\left[\|X - f_\theta\| - \|X\| \right] - \langle u, f_\theta \rangle \right\}.$$

Thus, θ_u^* is found by minimizing the cost functional that defines the spatial u-quantile, but the minimization is now performed only over the subset of $\mathcal{V}$ corresponding to the outputs of the model. It is interesting to notice that this cost

function takes into account the random nature of data in a natural way. As a consequence, the optimisation problem may yield better results than the bare reproduction of the target quantile through the model, namely the solution to a classic L^2-norm minimisation of model's error (see Section 3). Moreover, problem (**C**) is indexed by u, whose choice can be driven by the application. We will show an example of this in Subsection 3.1.

In practice, only the finite-dimensional, sample version of problem (**C**) can be considered, i.e:

$$(\widehat{\mathbf{C}}) \quad \widehat{\theta}_u^* := \arg\min_{\theta\in\Theta} \left\{ \frac{1}{N}\sum_{i=1}^{N} \left[\|X_i^{(n)} - f_\theta(t)^{(n)}\| - \|X_i^{(n)}\| \right] - \langle u^{(n)}, f_\theta(t)^{(n)} \rangle \right\}$$

where the superscript (n) indicates the projection onto a finite-dimensional subspace $\mathcal{V}_n \subset \mathcal{V}$. It is worth noticing that the whole dataset is employed in the definition of the cost functional, without parametric assumptions on data distribution. From a computational point of view, it can be solved with any reliable, global optimisation algorithm (for some examples, see Section 3).

2.2.3. *Measuring the Quality of the Calibration.* In order to have a measure of the quality of the calibration achieved by solving ($\widehat{\mathbf{C}}$), we consider the quantity:

$$B(u) = \left\| \frac{1}{N}\sum_{i=1}^{N} \frac{X_i^{(n)} - f_{\widehat{\theta}_u^*}(t)^{(n)}}{\left\| X_i^{(n)} - f_{\widehat{\theta}_u^*}(t)^{(n)} \right\|} + u^{(n)} \right\|, \tag{6}$$

which is the norm of the gradient of the spatial quantile cost functional (i.e. the sample version of problem (**Q**)) evaluated at the solution. $B(u)$ also has a statistical interpretation. It can be compared with a natural, standardised range of values, namely $0 \leq B(u) \leq 2$, that makes diagnostics arguments easy and interpretable. Here, values close to 2 indicate a calibration on the opposite direction of $u^{(n)}$, while values close to 0 correspond to good results.

When $u = 0$, the calibration problem targets the spatial median, and $B(0)$ can be interpreted in terms of statistical *spatial depth* (SD). Given a general r.v. X, we can define the spatial depth of a point $z \in \mathcal{V}$ as

$$SD(z; X) = 1 - \left\| \mathbb{E}\left[\frac{(z - X)}{\|z - X\|} \right] \right\|.$$

Given a dataset $X_1, \ldots, X_N$, its sample version becomes

$$\widehat{SD}(z; X) = 1 - \left\| \frac{1}{N}\sum_{i=1}^{N} \frac{(z - X_i)}{\|z - X_i\|} \right\|.$$

It is clear that SD ranges between 0 and 1 and reaches its maximum when z coincides with the spatial median of X. Therefore, statistical depths allow to introduce a center-outward order relation in high-dimensional data spaces where no natural order relation is available. They are completely non-parametric, easy to interpret and provide a natural range for comparisons.

In view of this, $B(0)$ can be interpreted as one minus the spatial depth of the optimised output with respect to the empirical distribution of X (Chakraborty

and Chaudhuri, 2014). Thus, it provides a standardised, meaningful and easy-to-interpret measure of *outlyingness*. When $u \neq 0$, (6) is no more a median-centric depth, but rather a quantile-centric depth of the optimised output. In any case, this quantity will only account for the quality of the calibration *per se*, serving as a measure of *model bias*, and not for the quality of the outcome of the minimisation algorithm used.

2.3. **The Dataset of Real ECGs.** The real data we use are part of a database created within the PROMETEO project (*PROgetto sull'area Milanese Elettrocardiogrammi Teletrasferiti dall'Extra Ospedaliero*). This project saw the collaboration of Azienda Regionale Emergenza Urgenza (AREU), Abbott Vascular and Mortara Rangoni Europe s.r.l., and was started by 118 Dispatch Center of Milan in the end of 2008, with the aim of spreading the intensive use of ECGs as pre-hospital diagnostic tool.

The standard ECG trace of a patient is composed of 12 records of the body surface electric potential. The data provided within PROMETEO project comprised eight records corresponding to leads I, II, $V1$, $V2$, $V3$, $V4$, $V5$ and $V6$. In the present work, we only consider lead I, which is widely used and allows us to assess the potentiality of the calibration procedure in a simpler framework. Moreover, we restrict the analysis only to healthy subjects, for a total of $N = 1588$ different signals.

Data were acquired in form of noisy, point-wise measurements ($P = 1200$ time points for each signal), and then pre-processed following standard procedures of functional data analysis (Ramsay and Silverman, 2005). First, they were smoothed and projected onto a suitable Fourier basis. Second, they were registered with the following landmarks: P-wave onset and offset, the QRS onset, the R peak, the QRS offset, the T peak and offset.

Registration, or alignment, is a standard step in the practice of functional data analysis accounting for the dispersion in time of the same features in the dataset. Since all inference is carried out under the assumption that the time-by-time comparison of signals is proper, we have to ensure that the same biological features happen at the same reference time. Healthy ECGs can be naturally registered by building a piecewise linear transformation constrained to map a set of landmarks to a reference grid of landmarks, i.e for each signal we compute: $\mathcal{H}_i : [0, T] \to [0, T]$,

$$s = \mathcal{H}_i(t) = \sum_{j=1}^{K} \left[\frac{t - l^i_{j-1}}{l^i_j - l^i_{j-1}} (\tilde{l}_j - \tilde{l}_{j-1}) + \tilde{l}_{j-1} \right] \mathbb{1}_t \left([l^i_j, l^i_{j-1}) \right),$$

$\forall i = 1, \dots, N$, where $\{0 = l^i_0, l^i_1, \dots, l^i_K = T\}$ indicates the original landmarks and $\{0 = \tilde{l}_0, \tilde{l}_1, \dots, \tilde{l}_K = T\}_j$ indicates the reference landmarks (for instance, the medians across the sample). The registered signals are given by $\widetilde{X}_i(s) = (X_i \circ \mathcal{H}_i^{-1})(s)$, $\forall i = 1, \dots, N$. A picture of the data at the different stages of the preprocessing is given in Fig. 2.

3. Results

In this section, the results of the calibration procedure are reported for the ODE and the PDE models.

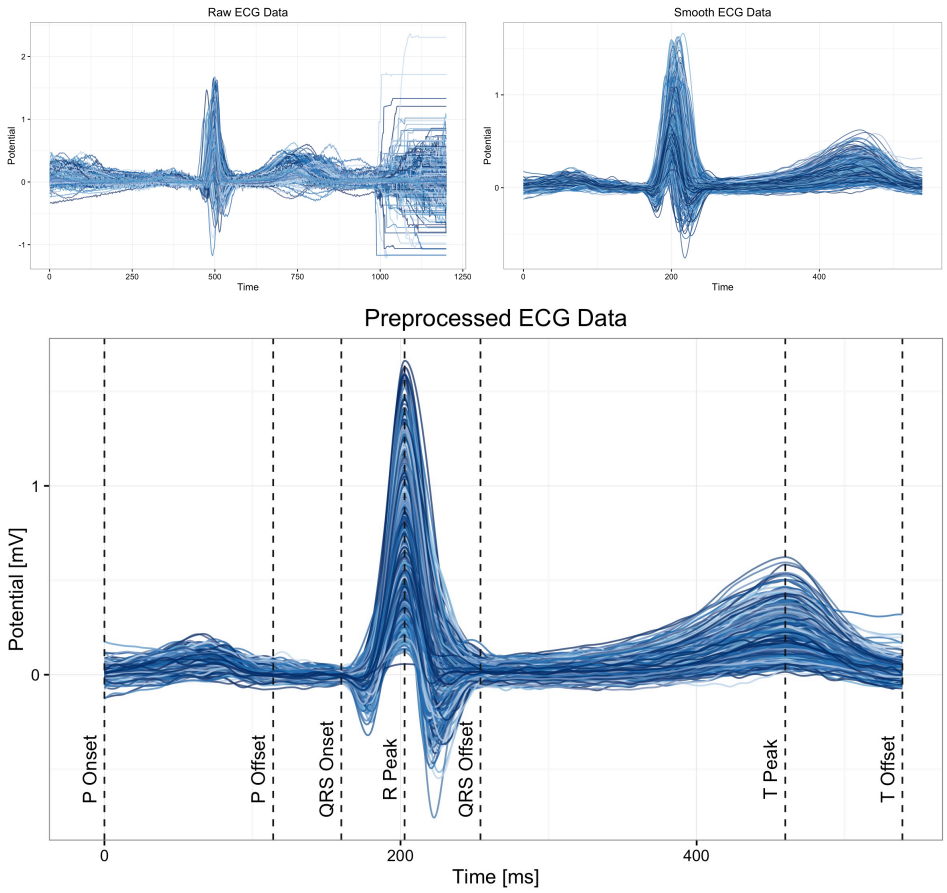

FIGURE 2. Real ECG signals, from raw data (top left), to smoothed (top right and bottom left) and registered data (bottom right).

TABLE 1. Values of calibrated set of parameters for ODE model

a_P	a_Q	a_R	a_S	a_T	b_P	b_Q	b_R	b_S	b_T
0.041	−0.045	0.704	0.107	0.008	0.184	5e-4	0.106	1e-10	0.523

3.1. **Calibration of the ODE Model.** We consider (1) as the model generating the synthetic profiles of ECGs and we search for the best set of parameters calibrating the model to the spatial median of the real ECG dataset. Among the 15 model parameters we fix $\theta_P, \ldots, \theta_T$ to the corresponding values of real functional data which, as described in Subsection 2.3, have been aligned via the corresponding landmarks. The 10 remaining parameters (a_i, b_i) are targeted by the minimisation problem ($\widehat{\mathbf{C}}$), which is solved through the L-BFGS-B optimisation algorithm implemented within the R (R Core Team, 2014) package `stats`, and able to deal with the positivity constraints of b_i's.

In order to highlight the robustness and effectiveness of the method, the optimisation step was initialized with an arbitrary set of parameters values. The results

are shown in Fig. 3. At the top of the figure, the initial guess, the calibrated output and the empirical spatial median are displayed, along with the data. We can see that the calibrated output and the spatial median are very similar. In the diagnostic plots we take advantage of the meaning of $B(0)$ and compare the spatial depth of the calibrated output with the empirical spatial depth of real data; we recall that the highest value of depth marks the empirical spatial median. It is clear that the calibrated output reaches a greater depth (i.e. is more central w.r.t the given dataset) than any other observation in the sample, spatial median included. This implies that by taking into account the whole set of data, a satisfactory result in terms of closeness to the true, unobserved, median can be reached; moreover, the outcome we get is even better than what would happen by calibrating the model to fit the empirical spatial median of the real dataset with a classic L^2-norm minimization problem, which in our case yields a spatial depth of the calibrated output of 0.511 (corresponding to the 86% quantile of the empirical distribution of spatial depth, which has to be compared to the 100% quantile obtained by solving $(\widehat{\mathbf{C}})$ as shown in Fig. 3). We report the value of calibrated parameters in Tab. 1.

Besides the calibration to the spatial median of data, we also targeted other quantiles in order to show the flexibility of the methodology. To do so, we considered the principal component (PC) decomposition of our dataset. Like in classic multivariate statistics, a principal component analysis (PCA) can be introduced for functional data, after defining a suitable analogue of variance-covariance structure for functions, i.e. the covariance operator. Functional PCs are the directions along which most of the variability of the process is expressed (for more details, see Ramsay and Silverman, 2005). The first one is generally the most important and in our application concerning real data it captures approximately 60% of the overall variability. It can be interesting then to calibrate the model to reproduce a selected set of quantiles along those directions, in order to capture that variability through the model. To do so, we compute the PCs $\{\varphi_i\}_{i=1}^{L}$, select the first, and set $u = c\varphi_1$, with $c = \pm\{0.083, 0.16, 0.25, 0.33, 0.416, 0.5\}$.

It must be noticed that the principal component basis can be used to parsimoniously represent both $X_i^{(n)}$'s, $f_\theta(t)^{(n)}$ and $u^{(n)}$ in problem $(\widehat{\mathbf{C}})$, only thanks to the peculiar translation-scale-rotation equivariance of spatial quantiles (Chaudhuri, 1996).

The results of the calibration procedure are displayed altogether in Fig. 4. When running the optimisation algorithm, we sorted the problems by (signed) increasing order of c_j, using as guess for the subsequent run of L-BFGS-B the result of the previous one. The values of $B(u)$ show a good quality of calibration as they are all between 0.15 and 0.26, with higher results corresponding to bigger values of c (which seems to be quite natural, as higher order quantiles are located farther away from the center of the data cloud, where data are sparser and inference is harder). By looking at Fig. 4, it can be seen how the ODE model, properly calibrated, is able to capture the variation of the median's shape expressed by φ_1, corresponding to the increasing order of quantiles.

By calibrating the model to several other quantiles than the median, one can draw

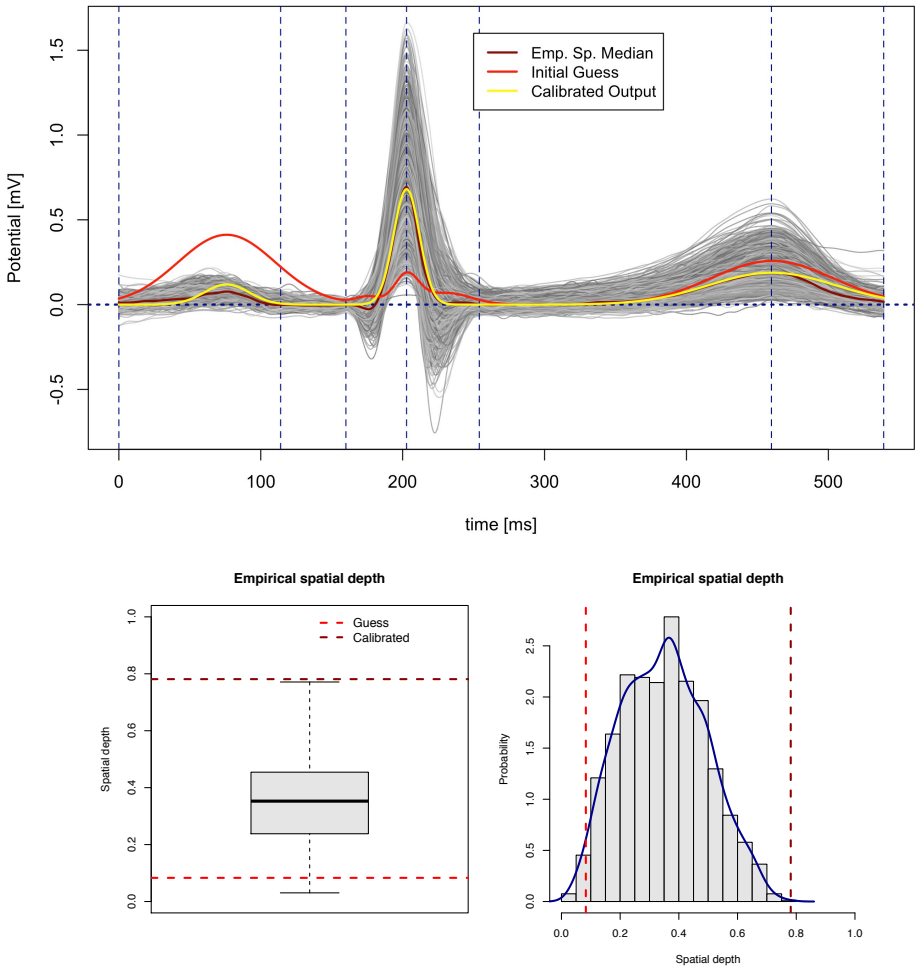

FIGURE 3. *Above:* Outcome of the calibration procedure to the spatial median ($u^{(n)} = 0$). *Below:* Diagnostics of the calibration.

level sets (or central regions) in the parameter space that produce spatial quantiles of a desired order. This, in turn, can be used directly to get both a summary of the variability ensuing from the variation in the parameters space, and to estimate the quantile order of model's output at a new set of parameters' values.

3.2. **Calibration of the PDE Model.** We applied the proposed calibration strategy to the PDE model described in Subsection 2.1.2. At first, we assessed the general quality of synthetic ECG obtained with the original parameters published in Schenone et al. (2015). In this article, the assessment was done by verifying that various biomarkers lay in the range found in the medical literature. Here we have a more systematic and quantitative approach by looking at the spatial depth of the signal with respect to the dataset of real ECGs. This allows us to quantify the quality of the synthetic signals in terms of centrality/outlyingness with respect to a real population. The graphics in Fig. 5 show that the original synthetic signals are

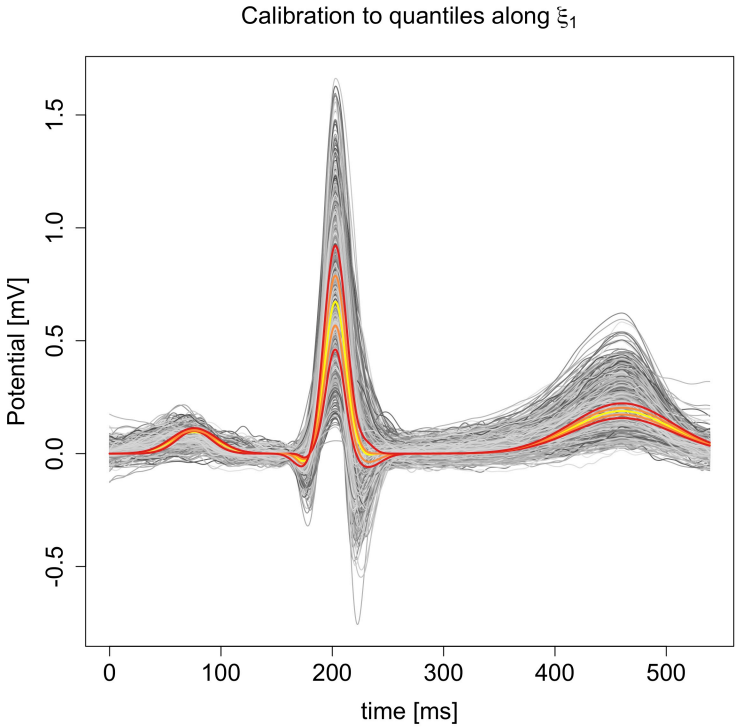

FIGURE 4. Output of the calibration of ODE model to general quantiles along first PC φ_1 (darker colours indicate calibration to higher order of quantiles, $\|u_i\| = |c_i|$, light yellow denotes the calibration to the median.).

almost always within the natural range of real data depths. But we can also see that their depths are too low to mark a well representative signal. We wish therefore to enhance the quality of model's output by calibrating it to the median of the real population.

In order to do so, among the many parameters involved in the composite PDE model, we choose g_{Na}^{PM}, g_{Na}^{CT} and g_{Na}^{BB} for Courtemanche-Ramirez-Nattel ionic model, and τ_{so_1} parameters in Minimum Ventricular model, which assumes 4 distinct values in epicardium, endocardium, M-cells and right ventricle, and it is such that $\tau_{so_1}^{endo} > \tau_{so_1}^{epi}$ (we refer to Courtemanche et al., 1998; Bueno-Orovio et al., 2008; Schenone et al., 2015 for the precise meaning of these parameters).

We then choose $u = 0$ and solve the optimisation problem $(\widehat{\mathbf{C}})$ for the values of the selected 7 parameters, where $f_\theta(t)^{(n)}$ is the PDE model's output at parameters θ, projected onto the first $n = 8$ principal components of the real dataset. The optimisation is carried out exploiting the efficient implementation of evolutionary algorithm CMA-ES (available within R through package `cmaes`), interfacing for each model's evaluation with the C++ parallel library FELiScE, solving the PDE model. In particular, at each iteration we: 1) evaluate the PDE model at parameters θ; 2) reconstruct the synthetic signal and align its landmarks to those of real data

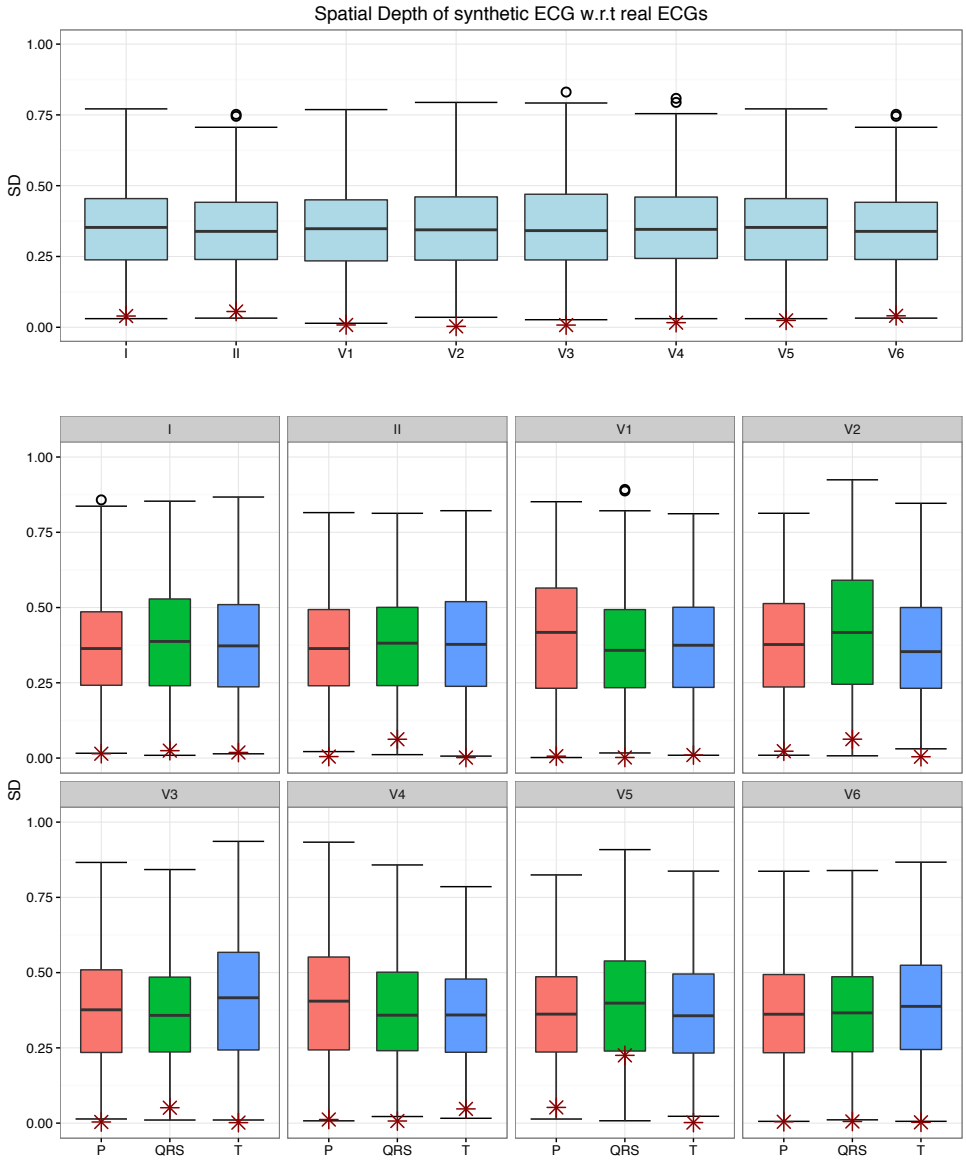

FIGURE 5. *Above*: Spatial Depths (SD) of original PDE-based ECG signal (red star), with respect to the real data (whose SD are displayed in the background boxplots), lead by lead. *Below*: SD of original PDE-based ECG signal (red star) with respect to real data, by lead and section (P, QRS and T wave).

(functional registration); 3) update the cost functional of problem ($\widehat{\mathbf{C}}$) and obtain the new parameter set for the next iteration.

At the end of the optimisation process, we obtain the results displayed in Fig. 6. By globally looking at the calibrated synthetic ECG signal, we can notice that the selected parameters mainly affect the vertical displacement inside S-T section, while the signal is practically unchanged in P- and QRS-wave.
In particular, the parameters influencing the atria dynamics, namely g_{Na}^{PM}, g_{Na}^{CT}

TABLE 2. Values of chosen parameters for calibrated PDE model

g_{Na}^{PM}	g_{Na}^{CT}	g_{Na}^{BB}	$\tau_{so_1}^{epi}$	$\tau_{so_1}^{endo}$	$\tau_{so_1}^{Mc}$	$\tau_{so_1}^{RV}$
14.508	27.378	47.112	19.15	30.17	45.19	19.56

and g_{Na}^{BB} does not seem to modify the shape of the P-wave in a way that drives the optimisation towards the selection of values yielding a better fit to data. On the contrary, the peak value of the T wave is successfully set to its correct value, determining a better fit of the model to the dataset's central tendency, and also the asymmetric shape of T wave is correctly reproduced. By looking at the boxplot of spatial depths (top right graphic in Fig. 6) we notice a slight rise in the value of depth for the synthetic signal, between initial and calibrated case. Such depth values are, respectively, 0.039 and 0.086.

The enhancement is clearer when looking at the only section that is affected by the calibration (bottom graphics in Fig. 6). In this case, if we truncate the time domain and compute again the spatial depths for the initial and calibrated synthetic signals, and for real data, we obtain a higher rise in data depth, from (respectively) 0.019 to 0.28. In particular, the calibrated S-T section is correctly situated within the bulk of real data (left graphic) and therefore its depth belongs to the central box of the boxplot. A summary of the values of parameters yielding this optimised output is given in Tab. 2 (the conductance parameters g_{Na}^{PM}, g_{Na}^{CT}, g_{Na}^{BB} are all expressed in $nS.pF^{-1}$, while τ_{so} parameters dimensionless).

4. DISCUSSION

The results displayed in Subsection 3.1 show a remarkably good ability of the proposed methodology to identify the set of parameters reproducing a desired functional target, be it the spatial median or other spatial quantiles. If we focus on the spatial median, the even low calibration error can be ascribed mainly to the inability of the model to reproduce asymmetric P and T waves.

When turning to the biophysical PDE model, results in Subsection 3.2 still show good results, even if with a smaller calibration gain. This is mainly due to the dramatically increased complexity of the model, and to the choice to focus on only a few parameters, for computational reasons. The results are still encouraging, and the enhancement in model's output is noticeable both visually (graphics on the left in Fig. 6) and quantitatively (graphics on the right in Fig. 6).

To this regard, the increase in optimal output's depth is less than what a visual comparison on signals would lead to, as spatial depths result from an overall measure of fit that cannot be split into time-by-time contributions. In other words, a shape twist in a time sub-interval of the synthetic signal would affect its depth as a whole, and to an extent not necessarily equal to the sub-interval's size. Other definitions of statistical depth, like Modified Band Depths (see Lopez-Pintado and Romo, 2007 and Lopez-Pintado and Romo, 2009), would average a scalar depth measure for each time point of the signal along the domain in order to determine the overall, functional depth. Therefore, if used to compute the depths of real and simulated signals that we obtained in our example, they would highlight a higher increment.

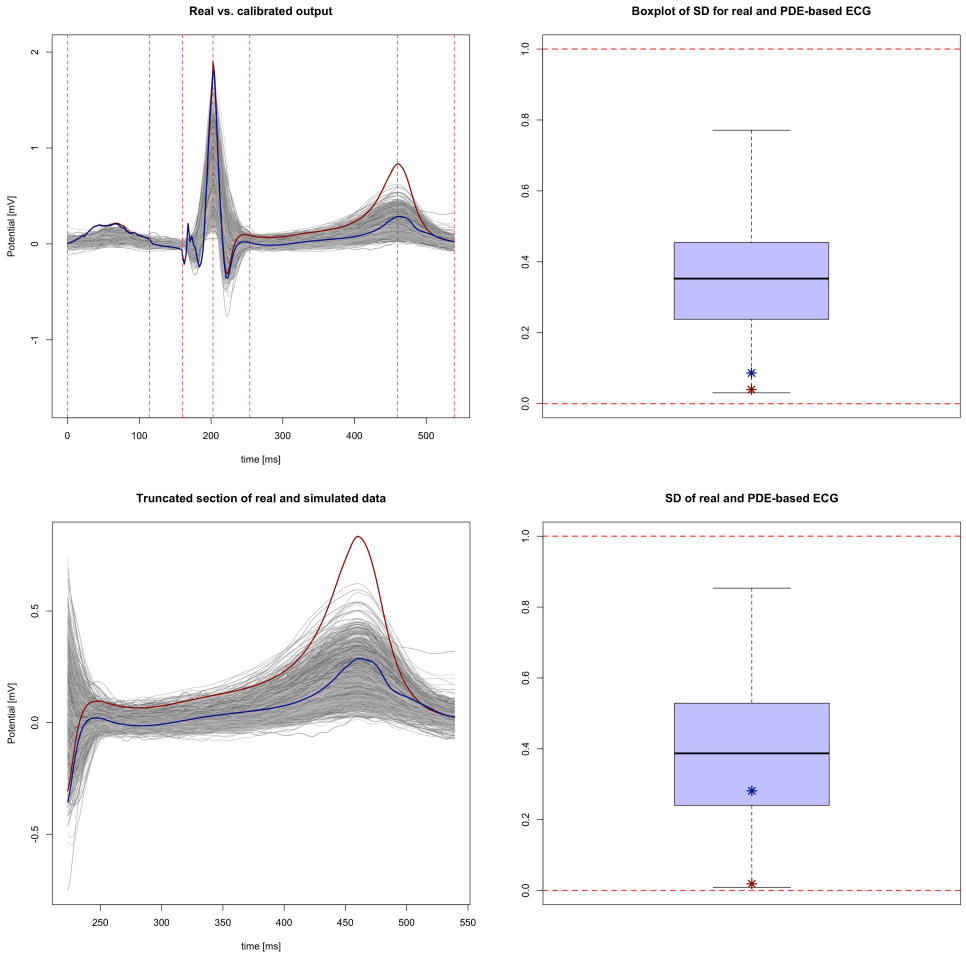

FIGURE 6. Outcome of the problem of calibrating the PDE model to the median of real data. *Above*: Initial synthetic signal (red) and optimised output (blue), compared to the real dataset (grey). *Below*: Comparison of synthetic initial and optimised signals with real data, only in the S-T segment.

5. CONCLUSION

We proposed and motivated a new calibration methodology based on statistical concepts, able to drive numerical models towards the reproduction of representative outputs with respect to a dataset of real data. Our applicative focus was on the calibration of numerical models for the production of synthetic ECGs, of which we described two possible instances based on ordinary or partial differential equations. We also introduced the notion of spatial quantiles and statistical depths, which are directly employed in the calibration methodology to provide a general, non-parametric and meaningful optimisation problem. In particular, we described in detail the interpretation of both the problem and the diagnostic quantities that can be used to assess the quality of its solution.

We applied this framework to the calibration of the two considered ECG models, exploiting a rich dataset of real measurements. In the ODE case we calibrated the

model to the spatial median of the dataset and to other quantiles along the first principal component, while in the PDE case we targeted the spatial median. For the ODE case, the values reported in Tab. 1 can be useful to people who use the model proposed in Clifford et al. (2005); McSharry et al. (2003) and who wants a synthetic healthy ECG calibrated on a real population.
For the PDE case, our procedure allowed us to assess and to improve the quality of the ECG obtained with the original parameters, in particular as far as the T-wave is concerned. The results we obtained, both from a qualitative and quantitative standpoint, support the flexibility and effectiveness of the proposed method, and pave the way to its application to different contexts and models.

References

Boulakia, M., Cazeau, S., Fernández, M., Gerbeau, J.-F., and Zemzemi, N. (2010). Mathematical modeling of electrocardiograms: a numerical study. *Annals of Biomedical Engineering*, 38(3):1071–1097.

Boulakia, M., Schenone, E., and Gerbeau, J.-F. (2012). Reduced-order modeling for cardiac electrophysiology. Application to parameter identification. *International Journal for Numerical Methods in Biomedical Engineering*, 28:727–744.

Bueno-Orovio, A., Cherry, E., and Fenton, F. (2008). Minimal model for human ventricular action potentials in tissue. *Journal of Theoretical Biology*, 253:544–560.

Buist, M. and Pullan, A. (2003). The effect of torso impedance on epicardial and body surface potentials: A modeling study. *IEEE Transactions on Biomedical Engineering*, 50(7):816 – 824.

Chakraborty, A. and Chaudhuri, P. (2014). The spatial distribution in infinite dimensional spaces and related quantiles and depths. *The Annals of Statistics*, 42(3):1203–1231.

Chapelle, D., Collin, A., and Gerbeau, J.-F. (2013). A surface-based electrophysiology model relying on asymptotic analysis and motivated by cardiac atria modeling. *Mathematical Models and Methods in Applied Sciences*, 23(14):2749–2776.

Chaudhuri, P. (1996). On a geometric notion of quantiles for multivariate data. *Journal of the American Statistical Association*, 91(434):862–872.

Clifford, G., Shoeb, A., McSharry, P., and Janz, B. (2005). Model-based filtering, compression and classification of the ecg. *International Journal of Bioelectromagnetism*, 7(1):158–161.

Collin, A., Gerbeau, J.-F., Hocini, M., Haïssaguerre, M., and Chapelle, D. (2013). Surface-based electrophysiology modeling and assessment of physiological simulations in atria. *FIMH 2013*, 7945:352–359.

Corrado, C., Gerbeau, J.-F., and Moireau, P. (2015). Identification of weakly coupled multiphysics problems. Application to the inverse problem of electrocardiography. *Journal of Computational Physics*, 283:271–298.

Courtemanche, M., Ramirez, R., and Nattel, S. (1998). Ionic mechanisms underlying human atrial action potential properties: insights from a mathematical model. *American Journal of Physiology*, 275(1):H301–H321.

Kemperman, J. (1987). The median of a finite measure on a banach space. *Statistical data analysis based on the L1-norm and related methods*, pages 217–230.

Koltchinskii, V. (1997). M-estimation, convexity and quantiles. *The Annals of Statistics*, 25(2):435–477.

Lopez-Pintado, S. and Romo, J. (2007). Depth-based inference for functional data. *Computational Statistics & Data Analysis*, 51(10):4957–4968.

Lopez-Pintado, S. and Romo, J. (2009). On the concept of depth for functional data. *Journal of the American Statistical Association*, 104(486):718 – 734.

Malmivuo, J. and Plonsey, R. (1995). *Bioelectromagnetism - Principles and Applications of Bioelectric and Biomagnetic Fields*. Oxford University Press.

Martin, V., Drochon, A., Fokapu, O., and Gerbeau, J.-F. (2012). Magnetohemodynamics in the aorta and electrocardiograms. *Physics in Medicine and Biology*, 57:3177–3195.

McSharry, P. E., Clifford, G. D., Tarassenko, L., and Smith, L. A. (2003). A dynamical model for generating synthetic electrocardiogram signals. *IEEE Transactions on Biomedical Engineering*, 50(3):289–294.

Potse, M., Dubé, B., and Gulrajani, R. (2003). ECG simulations with realistic human membrane, heart, and torso models. In *Engineering in Medicine and Biology Society, 2003. Proceedings of the 25th Annual International Conference of the IEEE*, volume 1, pages 70–73.

Potse, M., Dubé, B., and Vinet, A. (2009). Cardiac anisotropy in boundary-element models for the electrocardiogram. *Medical & biological engineering & computing*, 47(7):719–729.

Potse, M., Krause, D., Kroon, W., Murzilli, R., Muzzarelli, S., Regoli, F., Caiani, E., Prinzen, F., Krause, R., and Auricchio, A. (2014). Patient-specific modelling of cardiac electrophysiology in heart-failure patients. *Europace*, 16(suppl 4):iv56–iv61.

R Core Team (2014). *R: A Language and Environment for Statistical Computing*. R Foundation for Statistical Computing, Vienna, Austria.

Ramsay, J. O. and Silverman, B. (2005). *Functional Data Analysis*. Springer, New York, second edition.

Rincon, A., Bendahmane, M., and Ainseba, B. (2013). Computing the electrical activity of the heart with a dynamic inverse monodomain operator. In *2013 35th Annual International Conference of the IEEE Engineering in Medicine and Biology Society (EMBC)*, pages 3797–3800. IEEE.

Sachse, F. (2004). *Computational Cardiology: Modeling of Anatomy, Electrophysiology and Mechanics*. Springer-Verlag.

Schenone, E., Collin, A., and Gerbeau, J.-F. (2015). Numerical simulation of electrocardiograms for full cardiac cycles in healthy and pathological conditions. *International Journal for Numerical Methods in Biomedical Engineering*.

Sundnes, J., Lines, G., Cai, X., Nielsen, B., Mardal, K., and Tveito, A. (2006). *Computing the Electrical Activity in the Heart*, volume 1 of *Monographs in Computational Science and Engineering*. Springer-Verlag.

Trudel, M.-C., Dubé, B., Potse, M., Gulrajani, R., and Leon, L. (2004). Simulation of QRST integral maps with a membrane-based computer heart model employing parallel processing. *IEEE Transactions on Biomedical Engineering*, 51(8):1319–1329.

Wei, D., Okazaki, O., Harumi, K., Harasawa, E., and Hosaka, H. (1995). Comparative simulation of excitation and body surface electrocardiogram with isotropic and anisotropic computer heart models. *IEEE Transactions on Biomedical Engineering*, 42(4):343–357.

Politecnico di Milano, Via Bonardi 9, 20133 Milano (I)
E-mail address: nicholas.tarabelloni@polimi.it

MOX Off S.p.A., Via Durando 38/A, 20158 Milano (I)
E-mail address: elisa.schenone@moxoff.com

Inria Bordeaux and IMB, 351 cours de la Liberation, 33405 Talence (F))
E-mail address: annabelle.collin@inria.fr

Università degli Studi di Milano, via Saldini 50, 20133 Milano (I)
E-mail address: francesca.ieva@unimi.it

Politecnico di Milano, Via Bonardi 9, 20133 Milano (I)
E-mail address: anna.paganoni@polimi.it

Inria Paris and UPMC, 2 rue Iff, 75589 Paris (F)
E-mail address: jean-frederic.gerbeau@inria.fr

MOX Technical Reports, last issues

Dipartimento di Matematica
Politecnico di Milano, Via Bonardi 9 - 20133 Milano (Italy)

30/2016 Abramowicz, K.; Häger, C.; Pini, A.; Schelin, L.; Sjöstedt de Luna, S.; Vantini, S.
Nonparametric inference for functional-on-scalar linear models applied to knee kinematic hop data after injury of the anterior cruciate ligament

31/2016 Antonietti, P.F.; Merlet, B.; Morgan, P.; Verani, M.
Convergence to equilibrium for a second-order time semi-discretization of the Cahn-Hilliard equation

28/2016 Antonietti, P.F.; Dal Santo, N.; Mazzieri, I.; Quarteroni, A.
A high-order discontinuous Galerkin approximation to ordinary differential equations with applications to elastodynamics

29/2016 Miglio, E.; Parolini, N.; Penati, M.; Porcù, R.
GPU parallelization of brownout simulations with a non-interacting particles dynamic model

26/2016 Brunetto, D.; Calderoni, F.; Piccardi, C.
Communities in criminal networks: A case study

27/2016 Repossi, E.; Rosso, R.; Verani, M.
A phase-field model for liquid-gas mixtures: mathematical modelling and Discontinuous Galerkin discretization

25/2016 Baroli, D.; Cova, C.M.; Perotto, S.; Sala, L.; Veneziani, A.
Hi-POD solution of parametrized fluid dynamics problems: preliminary results

24/2016 Pagani, S.; Manzoni, A.; Quarteroni, A.
A Reduced Basis Ensemble Kalman Filter for State/parameter Identification in Large-scale Nonlinear Dynamical Systems

23/2016 Fedele, M.; Faggiano, E.; Dedè, L.; Quarteroni, A.
A Patient-Specific Aortic Valve Model based on Moving Resistive Immersed Implicit Surfaces

22/2016 Antonietti, P.F.; Facciola', C.; Russo, A.;Verani, M.
Discontinuous Galerkin approximation of flows in fractured porous media